Arab J Geosci (2014) 7:3281–3295
DOI 10.1007/s12517-013-1024-0

ORIGINAL PAPER

A modified rock physics model for analysis of seismic signatures of low gas-saturated rocks

Perveiz Khalid · Daniel Broseta · Dan Vladimir Nichita · Jacques Blanco

Received: 1 January 2013 / Accepted: 27 June 2013 / Published online: 9 July 2013
© Saudi Society for Geosciences 2013

Abstract In seismic applications, the bulk modulus of porous media saturated with liquid and gas phases is often estimated using Gassmann's fluid substitution formula, in which the effective bulk modulus of the two-phase fluid is the Reuss average of the gas and liquid bulk moduli. This averaging procedure, referred to as Wood's approximation, holds if the liquid and gas phases are homogeneously distributed within the pore space down to sizes well below the seismic wavelength and if the phase transfer processes between liquid and gas domains induced by the pressure variations of the seismic wave are negligible over the timescale of the wave period. Using existing theoretical results and low-frequency acoustic measurements in bubbly liquids, we argue that the latter assumption of "frozen" phases, valid for large enough frequencies, is likely to fail in the seismic frequency range where lower effective bulk modulus and velocity, together with dispersion and attenuation effects, are expected. We provide a simple method, which extends to reservoir fluids a classical result by Landau and Lifshitz valid for pure fluids, to compute the effective bulk modulus of thermodynamically equilibrated liquid and gas phases. For low gas saturation, this modulus is significantly lower than its Wood's counterpart, especially at the crossing of bubble point conditions. A seismic reflector associated to a phase transition between a monophasic and a two-phase fluid thus will appear. We discuss the consequences of these results for various seismic applications including fizz water discrimination and hydrocarbon reservoir depletion and CO_2 geological storage monitoring.

Keywords Rock physics · Low frequency · Seismic velocities · Thermodynamics · Fizz water · Fluid discrimination

P. Khalid (✉)
Institute of Geology, University of the Punjab,
54590 Lahore, Pakistan
e-mail: perveiz.geo@pu.edu.pk

D. Broseta · D. V. Nichita
Laboratory of Thermodynamics and Energetics of Complex Fluids,
Université de Pau, CNRS, BP1155, 64013 Pau Cedex, France

J. Blanco
Physeis Consultant, 23 route de Burosse, 64350 Lalongue, France

Introduction

Conventional seismic reflectivity measurements are very sensitive to the presence of a *free* gas phase, but not to its saturation in the reservoir rock. Low saturations of a *free* gas phase in an aquifer, commonly called "fizz" water, give rise to reflections as strong as those generated by high gas saturations (i.e., economic gas reservoirs), which is at the origin of a large number of drilled dry holes (Han and Batzle 2002). As another example, it is difficult to determine the exact position in the transition zone of the reflector associated to a gas/water or gas/oil contact. The quantitative description of the effects on seismic properties of partial substitution of liquid (oil or water) by gas is one of the most important challenges in seismic exploration and time lapse (4D) monitoring of reservoirs.

The poor sensitivity of seismic reflectivity to gas saturation is to a large extent captured within Gassmann's model (Gassmann 1951), in which the effective bulk modulus of the saturating two-phase (liquid and gas) fluid is approximated by the harmonic (or Reuss) average of the liquid and gas bulk moduli. This averaging procedure is often referred to as Wood's or as the effective medium approximation (Wood 1930). Within the above Gassmann–Wood model (GW), the P-wave velocity and impedance of porous rocks saturated with contrasted liquid and gas phases (such as water and gas in shallow reservoirs) are almost insensitive to gas saturation, except for low gas saturations. In a narrow interval of low gas saturations (S_g<5–10 %) these parameters vary rapidly but continuously between a minimum value reached for S_g~5–10 % and the maximum value corresponding to the fully water-saturated (S_g=0) rock.

Wood's approximation holds if two essential assumptions are satisfied. First, the liquid and the gas phases are homogeneously distributed within the pore space down to scales much smaller than the seismic wavelength. In other words, the wave frequency must be low enough and/or the liquid and the gas domains small enough compared to the wavelength. The second assumption, which is thoroughly discussed in this paper, is that the liquid and the gas phases remain "frozen" or *unrelaxed* at the passage of the seismic wave. We argue below that this assumption is very likely to break down in the seismic frequency band for typical reservoir and fluid settings.

In reality, mass transfer processes take place from one phase to the other when pressure varies at the passage of the seismic wave. In pure fluids, these processes consist in the condensation of the gas phase and in the vaporization of the liquid phase when pressure respectively increases or decreases. In multicomponent fluids, there is, in addition, a variation in phase composition, with the lighter components being transferred from the gas to the liquid phase (or vice versa) when pressure increases (or decreases). These processes are diffusive in nature and therefore act only when the wave frequency and/or the size of the phase domains are small enough. They induce relaxation between phases and therefore an increased effective compressibility or, equivalently, a lower effective bulk modulus. For very low frequencies and/or very small phase domains (quasistatic limit), the two fluid phases are thermodynamically equilibrated at any instant. This limit has been examined long ago by Landau and Lifshitz (1959), who calculated the *adiabatic* compressibility (i.e., the reciprocal of the bulk modulus) and sound velocity of a pure (i.e., one component) fluid at liquid/vapor equilibrium. Landau and Lifshitz obtained an effective bulk modulus for the *relaxed* (i.e., thermodynamically equilibrated) liquid and gas phases much lower than the effective bulk modulus of unrelaxed phases (Wood's modulus), especially for small proportions of the gas phase, i.e., near bubble point conditions. This modulus varies discontinuously at the crossing of phase boundaries (e.g., at bubble point conditions), in contrast to the continuous variation of Wood's modulus. Kieffer (1977) implemented the Landau–Lifshitz approach with water/steam systems in the context of volcanological and geothermal applications. Extensions of the Landau–Lifshitz analysis to multicomponent fluids have been recently proposed, for instance by Picard and Bishnoi (1987) and by Firoozabadi and Pan (2000). One important result is that strong discontinuities in the adiabatic compressibility and sound velocity of relaxed phases still exist at the crossing of bubble point conditions in multicomponent fluids, even though their amplitudes are less important than in the case of pure fluids. The discontinuity in adiabatic compressibility is reminiscent of that occurring for *isothermal* compressibility, which is well-known to reservoir engineers. For example, bubble point conditions are routinely determined in PVT laboratories from the angular point of the pressure vs. volume curve at constant temperature.

On the experimental side, it is well known that the presence of a minute amount of "free" gas in a liquid causes a dramatic decrease in sound velocity, together with an important attenuation. Temkin (1992) reports that air bubbles in a concentration by volume equal to 10^{-4} can decrease the speed of sound in water by 40 %. One application of this behavior is the early detection of vapor bubbles in liquid (Trammell 1962).

Our first purpose in this paper is to assess which of the above two regimes holds in representative reservoir/fluid systems and for seismic frequencies (from 1 to 10^4 Hz). Is it Wood's regime of unrelaxed fluid phases, as is commonly assumed, or the Landau–Lifshitz low-frequency regime of relaxed phases or an intermediate dispersive regime?

In this paper, we focus on low gas-saturated reservoirs, in which the differences between the relaxed and unrelaxed bulk moduli for the saturating two-phase fluid turn out to be the largest. Low gas-saturated reservoirs are encountered for instance in the exploration stage (see above the discussion on "fizz" water) or in the production stage as a result of a pressure drawdown below the fluid's bubble point pressure. In reservoirs containing initially (i.e., at discovery) an undersaturated oil, this drawdown is responsible for the apparition of secondary gas caps and oil/gas contacts. The saturation state consists in gas bubbles sparsely and homogeneously distributed within the liquid (oil or water). Such low gas-saturated states are stable (i.e., the gas is immobile in the porous medium) as long as gas saturation does not exceed to the so-called critical gas saturation, which is usually larger than 10 % for typical rock/fluid systems.

This saturation state is akin to that in a bubbly liquid, in which gas bubbles are sparsely and homogeneously dispersed in the liquid and bubble dimensions do not exceed a few microns (i.e., the maximum pore size in most rocks). The low-frequency acoustic behavior of bubbly (pure) fluids has been the subject of a number of theoretical (Onuki 1991) and experimental studies (Coste et al. 1992; Coste and Laroche 1993). These studies, which complemented earlier studies by Soviet scientists, are used in this paper to gain insight into the seismic behavior of low gas-saturated reservoirs. Besides the presence of a rock phase, fluid composition is the most important difference between the pure (i.e., one component) fluid situation investigated by Onuki (1991) and Coste et al. (1992) and the multicomponent reservoir fluids of interest here. In the seismic frequency band ($1–10^4$ Hz), our analysis shows that Wood's approximation of "frozen" (or unrelaxed) fluid phases is not likely to hold for describing the compressive (and acoustic) behavior of typical reservoir liquids with a small amount of gas bubbles. This is the main result of this paper, which justifies an examination of the

"thermodynamic" (Landau–Lifshitz) limit of relaxed fluid phases and its impact on the seismic behavior of saturated rocks.

The paper is organized as follows. The next section is a reminder of the conventional Gassmann–Wood model for the saturation dependence of the bulk modulus and P-wave velocity of a partially saturated porous medium. In the following section, we question Wood's assumption of "frozen" (or unrelaxed) fluid phases on the basis of the current knowledge on the acoustic properties of bubbly liquids and we end up with the conclusion that this assumption might not be verified in the seismic frequency band for typical reservoir rocks saturated with a liquid (e.g., water or oil) and a small amount of homogeneously dispersed gas bubbles.

A section is then devoted to the "thermodynamic" (or Landau–Lifshitz) limit of relaxed fluid phases and a comparison of this limit to the conventional (Wood) regime. A simplified scheme is proposed for calculating the "thermodynamic" compressibility of the saturating two-phase fluid, which is implemented on various reservoir/fluid systems: one contrasted hydrocarbon fluid and two aqueous fluids containing either CO_2 or methane, the latter system being representative of fizz water. At low gas saturation (i.e., close to bubble point conditions), the "thermodynamic" compressibility turns out to be significantly higher than that obtained within the standard Wood's approach, which leads to a lower bulk modulus and P-wave velocity of the saturated reservoir rocks. Finally, we present a preliminary analysis of the impact of these differences on seismic traces, as well as practical implications relating to fizz water discrimination and 4D seismic monitoring of producing hydrocarbon reservoirs and CO_2 geological storage in deep aquifers.

Rocks saturated with unrelaxed fluid phases: the Gassmann–Wood model

To estimate fluid saturation effects on seismic wave velocities, Gassmann's fluid substitution model is often used in combination with Wood's expression for the effective bulk modulus of the saturating two-phase fluid. Gassmann's equation relates the bulk modulus of the fluid-saturated rock, K_{sat}, to the bulk modulus of the drained (or dry) rock, K_{dr}, to that of the rock-forming mineral, K_m, and to the adiabatic (or isentropic) bulk modulus of the saturating fluid, K_f:

$$K_{\mathrm{sat}} = K_{\mathrm{dry}} + \alpha^2\left[\frac{\phi}{K_f} + \frac{\alpha-\phi}{K_m}\right]^{-1} \approx K_{\mathrm{dry}} + \frac{\alpha^2}{\phi}K_f \qquad (1)$$

where $\alpha=1-K_{dr}/K_m$ is Biot's coefficient and ϕ is rock porosity. K_f is related to fluid density ρ_f and sound velocity c_f: $K_f=\rho_f c_f^2$. Gassmann's equation is applicable when (1) the rock and its forming mineral(s) are isotropic and homogeneously distributed, (2) all pores are hydraulically connected, and (3) there is no relative motion between fluid and solid, which requires that the wave frequency be low enough (this condition is usually satisfied in the seismic band). The expression on the right-hand side of Eq. 1 is an approximation of the bulk modulus K_{sat} valid for high porosities (ϕ>15 %; Han and Batzle 2004; Zinszner and Pellerin 2007).

The P-wave velocity in the fluid-saturated porous rock is given by

$$V_p = \left(\frac{K_{\mathrm{sat}} + 4\mu/3}{\rho}\right)^{1/2} \qquad (2)$$

where $\rho=(1-\phi)\,\rho_m+\phi\rho_f$ is the density of the saturated rock (ρ_m and ρ_f being the mineral and fluid densities, respectively), and μ is the rock shear modulus (μ is independent of the nature and amount of saturating fluids in Gassmann's model).

When two fluid phases (e.g., a gas phase and a liquid phase such as water or oil) are present in the rock, they are assimilated to a single fluid with effective density $\rho_f=S_l\rho_l+S_g\rho_g$, where S_l and $S_g=1-S_l$ are the volume fractions or saturations of the liquid and gas phases. Wood's approximation states that the modulus K_f is the Reuss (isostress) average of the adiabatic bulk moduli of the gas and liquid phases, noted K_g and K_l, respectively:

$$K_f = \left(\frac{S_g}{K_g} + \frac{S_l}{K_l}\right)^{-1} \qquad (3)$$

Wood's Eq. 3 follows from the definition of K_f, which is the reciprocal of the adiabatic compressibility β_f of the two-phase (liquid and gas) fluid, i.e.,

$$\begin{aligned}\beta_f &= -\frac{1}{V_l+V_g}\left(\frac{\partial\left(V_l+V_g\right)}{\partial P}\right)_S \\ &= -\frac{V_l}{V_l+V_g}\frac{1}{V_l}\left(\frac{\partial V_l}{\partial P}\right)_S - \frac{V_g}{V_l+V_g}\frac{1}{V_g}\left(\frac{\partial V_g}{\partial P}\right)_S\Big\} \\ &= \frac{S_l}{K_l}+\frac{S_g}{K_g} = S_l\beta_l + S_g\beta_g\end{aligned} \qquad (4)$$

where V_l and V_g are the liquid and gas volumes and subscript S means that the partial derivatives are taken at constant entropy (adiabatic conditions). In Eq. 4, the quantities $\beta_l=1/K_l=1/\rho_l c_l^2$ and $\beta_g=1/K_g=1/\rho_g c_g^2$ are the adiabatic compressibilities of the liquid and gas phases, respectively, c_l and c_g being the sound velocity in the liquid and gas phases.

There are two underlying assumptions in the derivation of Wood's Eqs. 3 and 4 (Batzle and Wang 1992). First, the pressures in the liquid and the gas phases are equal (isostress conditions), which means that the phase domains are homogeneously distributed and small compared to the wavelength

of the acoustic wave. In other words, the wave frequency must be low enough. Second, the liquid and gas phases are "frozen", i.e., they do not have enough time to exchange matter at the passage of the pressure wave. This assumption holds only if frequency is high enough and/or phase domains are small enough. We discuss in the next section the range of applicability of Wood's approximation.

For completeness, it is worth mentioning here that, when the first assumption is not satisfied (i.e., when the liquid and the gas phases form patches not small compared to the wavelength of the acoustic wave, which occurs for instance for high enough frequencies), the effective bulk modulus of the two-phase fluid K_f is higher than Wood's modulus (Eq. 3). Wood's model thus provides a lower bound for the modulus K_f only if the assumption of "frozen" (or unrelaxed) phases is satisfied. As we will see below, lower values than Wood's are obtained when frequency (or phase domains) are small enough to allow transfer processes to take place between the liquid and gas domains.

When calculated within the Gassmann–Wood model, the P-wave velocity of porous rocks saturated with liquid and gas (or vapor) displays very characteristic saturation dependences. For reasonable rock parameters and contrasted fluid phases (e.g., $K_g/K_l<10^{-2}$, as is often the case with water and gas in shallow reservoirs), the velocity V_P first decreases sharply, but continuously, with increasing S_g, before reaching a minimum value for S_g~5–10 %, and then it increases slowly with S_g. For lower contrasts between liquid and gas, as is the case between water and gas in deep gas reservoirs, these trends are less pronounced, and the minimum of the velocity V_P is shifted to higher gas saturations (Han and Batzle 2002).

Breakdown of Wood's model for low gas-saturated rocks in the seismic frequency band

We are concerned here with the seismic behavior of rocks saturated with a liquid (water or oil) and a small amount of gas bubbles homogeneously dispersed in the pore space. This saturation state is encountered for instance when a water- or oil-bearing reservoir is drawn down below bubble point pressure. The dissolved gas then comes out of solution and forms a distinct phase, whose saturation increases with decreasing pressure. At the microscopic scale, low gas-saturated reservoirs are often characterized by gas bubbles sticking to the pore walls, albeit with a high contact angle, the liquid being usually the most wetting phase. A significant proportion of their surface is therefore in contact with the liquid. It is reasonable to assume that this phase distribution has acoustic properties equivalent to those of a bubbly fluid with similar gas volume fraction and bubble sizes not exceeding a few microns (that is, the maximum pore size in most reservoir rocks).

The acoustic properties of a bubbly *pure* (i.e., one component) fluid have been extensively studied, both theoretically (Onuki 1991) and experimentally (Coste et al. 1992; Coste and Laroche 1993), for frequencies much lower than the resonance frequency of the individual gas bubbles (which is typically much larger than tens of kilo-Hertz for submicron-sized bubbles). At the passage of the pressure wave, the phase equilibrium between liquid and gas (called vapor when in thermodynamic equilibrium with the liquid) is perturbed: condensation of some of the vapor (at pressure peaks) or vaporization of some of the liquid (at pressure troughs) take place at liquid/gas interfaces, where therefore latent heat is generated. The actual state—relaxed or unrelaxed—of the bubbly fluid is determined by the relative values of two characteristic timescales: the timescale required for the perturbed system to reach a new equilibrium state and the sampling time, i.e., the period of the acoustic wave. In pure fluids, the former timescale is controlled by heat diffusion: liquid/vapor equilibrium is attained if enough time is left for the latent heat to be removed from, or brought to, the liquid/gas interfaces by heat diffusion. For dilute vapor bubbles in a liquid, the liquid acts as a heat bath, providing heat to, or removing it from, the liquid/vapor interfaces by conduction. From a detailed analysis of these heat and mass transfer processes, Onuki (1991) derived an expression for the frequency dependence of the adiabatic compressibility of pure fluids in two-phase (i.e., liquid and gas) conditions. This expression reduces to the Landau–Lifshitz' (relaxed) value at low enough frequency and to Wood's (unrelaxed) value at high enough frequency. The resonance, or maximum attenuation, occurs for a characteristic frequency f_c such that the thermal diffusion length in the liquid phase $(D_l/2\pi f_c)^{1/2}$ is of the order of the mean distance between vapor bubbles $l \approx R/S_g^{1/3}$, where D_l is the liquid thermal diffusivity and R is the radius of the gas bubbles. This characteristic frequency is thus given by:

$$f_c \approx D_l/l^2 \approx D_l S_g^{2/3}/R^2 \tag{5}$$

This simple scaling argument is due to Coste and Laroche (1993) who checked the consistency of Eq. 5 with the maximum attenuation extracted from Onuki's dispersion relation. If the frequency of the acoustic wave f is much higher than the characteristic frequency f_c, the two-phase fluid behaves as a "frozen" or unrelaxed fluid system, and its effective bulk modulus is given by Wood's value (Eq. 3). If f is much lower than the characteristic frequency f_c, then the two-phase fluid is in a relaxed state (i.e., in thermodynamic equilibrium) at any instant and its effective bulk modulus is given by the Landau and Lifshitz expression (1959).

On the experimental side, we are aware of a set of low-frequency acoustic measurements in liquid diethyl ether containing a low fraction (S_g<1 %) of vapor bubbles with radius R ~1 mm (Coste et al. 1992; Coste and Laroche 1993). The measurements consisted in observing the standing-wave behavior of a Helmholtz resonator filled with the bubbly liquid that allowed resonant frequencies as low as a few Hertz to be investigated. Coste and his coworkers showed clear evidence for the failure of Wood's effective medium model, manifested by strong attenuation effects due to the liquid/vapor transition, even though frequencies were quite higher than the characteristic frequency f_c, equal to a few milli-Hertz for that particular system.

The theoretical arguments and the measurements summarized above are for pure (i.e., one component) fluids, in which the approach to thermodynamic equilibrium is kinetically controlled by heat diffusion. The reservoir fluids of interest in this paper are not pure fluids, but multicomponent mixtures containing at least two components. The approach to equilibrium is then a more complex dynamical process, involving also diffusive transport of the different components from one phase to the other across the interfaces between phases. A simplification occurs when the fluid can be described by only two components (or pseudocomponents) with contrasted volatilities: one nonvolatile component, hence present only in the liquid phase, and one volatile (light) gas component present in both gas and liquid phases. This description, which reservoir engineers refer to as the "black oil" model, is applicable to a large number of reservoir fluids, including contrasted hydrocarbon mixtures and aqueous fluids (see next section for a more thorough presentation of this model). Under thermodynamic equilibrium conditions, a pressure increase (or decrease) is accompanied by an increase (or decrease) in the amount of dissolved gas component in the liquid. The gas component, in addition to heat, therefore goes back and forth across the liquid/gas interface at the passing of the pressure wave. The rate-controlling factor that governs the approach to thermodynamic equilibrium in such fluid systems is the diffusivity of the light (or gas) component in the liquid, because this is the slowest process: gas diffusion coefficients in liquids are one or two orders of magnitude lower than typical liquid thermal diffusivities. For instance, the diffusivities of methane or CO_2 in water are in the range of 10^{-8}–10^{-9} m^2/s (in a porous medium the effective diffusivity is still lower by a factor equal to the tortuosity), whereas thermal diffusivities of liquids such as water or diethyl ether are rather in the range of 10^{-7} m^2/s (Coste et al. 1992). The pure-fluid analysis by Onuki (1991) and Coste et al. (1992, 1993) is still applicable, but liquid thermal diffusivity should be replaced by gas diffusivity in Eq. 5. Then, for gas bubble sizes typically encountered in low gas-saturated porous media, smaller than the millimetric bubbles in Coste's experiments by, say, 3 or more orders of magnitude, we end up for comparable gas saturations (S_g approximately a few parts per thousand) with a characteristic frequency f_c higher by at least 4 orders of magnitude than that corresponding to Coste's experiments (equal to a few milli-Hertz, see preceding paragraph). Hence, in the seismic frequency band, Wood's assumption of "frozen" phases is likely to break down.

The above analysis holds provided gas bubbles are rather homogeneous in sizes and homogenously dispersed in the pore space. In a porous medium, this corresponds to a saturation state arising typically from a depletion process, whereas a gas displacement process would lead to a less uniform (i.e., more patchy) phase distribution. In addition, Onuki (1991) and Coste et al. (1992, 1993) considered bubble sizes large enough to neglect capillary pressure effects, i.e., effects related to the pressure difference between gas and liquid. These effects have been examined in the thermodynamic limit by Firoozabadi and Pan (2000). Near bubble point pressure conditions, they are found to be negligible if the overpressure in the gas phase does not exceed a few bar, which corresponds to gas bubbles larger than about 0.1 μm. Lastly, the thermal influence of the solid matrix making up the porous medium on the saturating fluid has been neglected (i.e., pore walls are considered to be adiabatic: no heat is transferred between the solid matrix and the fluid at the passage of the seismic wave). This assumption is implicit in the standard Gassmann model. In reality, some heat transfer takes place across mineral/fluid interfaces at the passage of the pressure wave, whose effect is to increase the effective compressibility of the saturating fluid towards a value intermediate between the adiabatic and isothermal fluid compressibilities. For the class of fluids examined in this paper, however, it turns out that there are very little differences between the adiabatic and isothermal compressibilities (see next section).

To conclude this section, the available theoretical and experimental evidences suggest that the standard Wood procedure might not be applicable in the seismic frequency band for evaluating the effective compressibility or bulk modulus of two-phase (liquid and gas) contrasted ("black oil") fluids saturating a typical porous rock, at least for low gas saturations (i.e., close to bubble point pressure conditions). This modulus, an essential ingredient in Gassmann's fluid substitution model, is therefore examined in the thermodynamic limit in the next section.

Rocks saturated with relaxed fluid phases: the Gassmann–Landau and Lifshitz model

We refer to the regime in which the liquid and gas phases can be considered as fully relaxed or thermodynamically equilibrated at the passage of the seismic wave as the thermodynamic or Landau–Lifshitz regime. In this regime, the

compressibility of the two-phase fluid is higher than in Wood's regime, where the fluid phases behave as "frozen" (or unrelaxed) phases. In the following, we propose a simplified method to compute the "thermodynamic" (or relaxed) two-phase compressibility, which is appropriate for the class of reservoir fluids obeying the "black oil" (BO) description. We then implement this method on three typical reservoir fluids, including one hydrocarbon mixture and two aqueous fluid systems, and we calculate by means of Gassmann's formula (Eq. 1) the bulk modulus and P-wave velocity of a given porous rock (representative of a porous and poorly consolidated sand) saturated with those two-phase fluid systems. The latter modulus and P-wave velocity are compared to those obtained within the conventional Gassmann–Wood model.

BO approximation of two-phase compressibility

In the BO approach, the reservoir fluid is described by two components (or pseudocomponents): one is nonvolatile and, therefore, present only in the liquid phase, and the other is volatile and may be present both in the liquid phase (as a dissolved or associated gas) and in the "free" gas phase. The liquid phase is conventionally called oil, but this liquid phase can be water as well. The BO parameters of a given reservoir fluid at fixed temperature T and pressure P are:

1. The volume ratio of liberated gas to remaining liquid at standard conditions (288 K and atmospheric pressure), or solution gas–liquid ratio, denoted R_s.
2. The liquid and gas formation volume factors, denoted by B_l and B_g, respectively, equal to the volume of liquid and gas at T and P, relative to the volume at standard conditions.

These parameters are determined directly from PVT measurements usually carried out in the laboratory under isothermal conditions or by using simple methods or correlations such as those proposed by Batzle and Wang (1992). The isothermal compressibility β_f of the single-phase liquid (P is higher than bubble point pressure P_b) is

$$\beta_{f,\mathrm{BO}} = -\frac{1}{B_l}\left(\frac{\partial B_l}{\partial P}\right)_T \tag{6}$$

and that of the two-phase fluid with gas and liquid saturations S_g and S_l ($P<P_b$), is (see, e.g., McCain 1990)

$$\beta_{f,BO} = S_l\left[-\frac{1}{B_l}\left(\frac{\partial B_l}{\partial P}\right)_T + \frac{B_g}{B_l}\left(\frac{\partial R_s}{\partial P}\right)_T\right] + S_g\left[-\frac{1}{B_g}\left(\frac{\partial B_g}{\partial P}\right)_T\right] \tag{7}$$

The expression in the right-hand side bracket of Eq. 7 is the gas phase compressibility and that in the left-hand side bracket is the liquid phase compressibility, in which the second term accounts for the gas evolving from the liquid under a pressure variation. From Eqs. 6 and 7, it appears that there is a discontinuity in the fluid compressibility at the crossing of bubble point pressure P_b:

$$\Delta\beta_{f,BO} = \left(\frac{B_g}{B_l}\frac{\partial R_s}{\partial P}\right)_{T,P=P_b} \tag{8}$$

This expression can be rewritten in terms of the equilibrium molar fraction of the gas dissolved in the liquid phase x, and the molar volumes V_g and V_l of the gas and liquid at T and P_b:

$$\Delta\beta_f \approx \left(\frac{V_g}{V_l}\frac{\partial x}{\partial P}\right)_{T,P=P_b} \tag{9}$$

where use has been made of the definitions of $B_g = V_g/V_{g,\mathrm{st}}$, $B_l = V_l/V_{l,\mathrm{st}}$ and $R_s = xV_{g,\mathrm{st}}/(1-x)V_{l,\mathrm{st}} \approx xV_{g,\mathrm{st}}/V_{l,\mathrm{st}}$, where subscript st represents standard conditions and x is usually a small quantity. The meaning of Eqs. 8 and 9 is the following. Consider one mole of liquid containing a small amount of "free" gas (i.e., P is slightly lower than P_b) with total volume $V \approx V_l$, and let the pressure vary from P to $P+\mathrm{d}P$. The total volume then varies by an amount equal to $dV = V_g dx = V_g(x(P+dP)-x(P))$ corresponding to the volume lost (or gained) by gas dissolution into (or exsolution from) the liquid phase when pressure increases (or decreases). This variation, which is absent in Wood's description, comes in addition to that of the liquid phase. The link between $\Delta\beta_f$ (the compressibility enhancement with respect to Wood's compressibility) and the gas solubility behavior is thus clearly established. This link is still clearer if we examine the low-pressure behavior of Eqs. 8 and 9. At low pressure $V_g = \mathrm{RT}/P$ (ideal gas law), where R is the perfect gas constant and gas solubility increases linearly with pressure, i.e., it follows Henry's law, $x = P/H$, where Henry's law constant H is specific to a given liquid/gas system and is temperature-dependent (tabulations of $H(T)$ are available in the literature for the most common liquid/gas systems). Hence, when the bubble point pressure is sufficiently low (say, below a few bar to a few tens of bar, depending of the liquid/gas system and temperature), the compressibility jump $\Delta\beta_f$ at the crossing of bubble point pressure P_b is equal to

$$\Delta\beta_f \approx \frac{1}{H(T)}\frac{\mathrm{RT}}{P_b V_l} \tag{10}$$

The compressibility enhancement thus decreases with increasing pressure and decreasing Henry's law constant, i.e., with decreasing gas solubility. These trends persist at higher pressures, as shown in the analysis of the compressive behavior of various reservoir fluid systems presented below.

The previous equations in this section provide isothermal compressibilities, whereas the compressibilities of interest

are adiabatic ones. In the case of reservoir fluids obeying the "BO" description, the difference between isothermal and adiabatic compressibilities is negligible, both in the one-phase (liquid) region and in the two-phase region, provided the amount of gas phase is small, and Eqs. 6 to 8 thus provide a good approximation of the latter compressibilities. In the case of the reservoir fluid examples examined below, this statement can be substantiated by an extensive calculation of both isothermal and adiabatic compressibilities, which only require an equation of state for the fluid system (Nichita et al. 2010). The results from this calculation serve here as a benchmark for our simplified BO approach.

We will envisage two evolutions of reservoir fluid conditions. In one of these, the reservoir fluid with fixed temperature T and composition undergoes a pressure variation across the bubble point pressure P_b marking the boundary between the monophasic (liquid) state ($P>P_b$) and the two-phase (liquid and gas) conditions ($P<P_b$). This corresponds for instance to a depletion process (drawdown) in a reservoir. The liquid saturation S_l ($P<P_b$) is related to the BO parameters as follows:

$$S_l(T,P) = \left(1 + B_g\left(R_s(T,P_b) - R_s(T,P)\right)/B_l\right)^{-1} \qquad (11)$$

The other useful description of fluid conditions is in terms of S_g, all other conditions such as reservoir temperature and pressure being fixed. Fluid compressibility variations are obtained by letting S_g and $S_l = 1 - S_g$ vary in Eqs. 6 and 7, in which the other quantities are estimated at the temperature and pressure of interest. This description, in which only the fluid composition varies, is for instance needed for inferring saturation maps from seismic reflectivity data.

Examples

The three chosen examples consist in the same porous medium saturated with three different reservoir fluids. The porous medium has properties similar to those of the Utsira sands in the North Sea, namely a quartzitic sand with porosity ϕ=34 %, Biot's coefficient $\alpha \approx 0.92$, and dry rock bulk modulus $K_{\mathrm{dry}} \approx 2.8$ GPa (Arts et al. 2004). One fluid is a contrasted hydrocarbon mixture well-documented in the literature (Stenby et al. 1996; Nichita et al. 2007), which is in two-phase (i.e., oil and gas) conditions at the reservoir temperature of 344 K. Its bubble point pressure is equal to 298 bar. The other two fluids are mixtures of water and a soluble gas, either carbon dioxide (CO_2) or methane (CH_4), under typical shallow offshore conditions; they are representative of fluids resulting from CO_2 injection in a shallow offshore aquifer (Arts et al. 2004) and of "fizz" water (Han and Batzle 2002). The calculation of the bulk modulus and P-wave velocity of the saturated rock is carried out in two steps. First, the method described in the previous subsection is utilized for calculating the compressibility of the saturating two-phase fluid. Then Gassmann's formula and Eq. 2 are used to compute the bulk modulus and P-wave velocity of the saturated rock, which are compared to those obtained within the conventional Gassmann–Wood method.

Hydrocarbon-bearing reservoir

The porous medium (see preceding paragraph) is saturated with a live oil having a bubble point pressure P_b=298 bar at reservoir temperature T=344 K. This oil is a contrasted hydrocarbon fluid with an associated gas consisting essentially of methane; its composition, together with the parameters of the Peng and Robinson (1976) equation of state that best match the PVT data, are reported in Stenby et al. (1996) and in Nichita et al. (2007). The process of interest here is a depletion process (or drawdown), in which pressure varies from above P_b (one-phase region) to below P_b (two-phase region) at constant T=344 K. The BO parameters of this fluid in the one-phase region ($P>P_b$), i.e., $B_l(P)$, and in the two-phase region ($P<P_b$), i.e., $B_g(P)$, $B_l(P)$, and $R_s(P)$, are taken from Nichita et al. (2007); in particular, the solution gas–oil ratio of the monophasic oil at P_b is equal to $R_s(P_b)$=110 l of gas per liter of oil (at standard conditions). The fluid compressibility in the one-phase (i.e., oil) region slightly above P_b ($P>P_b$), calculated by Eq. 6, is represented in Fig. 1 by the circle on the S_l=1 axis. The compressibility in the two-phase (i.e., oil and gas) region ($P<P_b$) calculated from Eqs. 7 and 11 is also depicted in Fig. 1 as a function of liquid saturation S_l, with S_l varying from 1 to 0.95 or S_g varying from 0 to 0.05 (corresponding to a drawdown from P_b=298 bar to P=255 bar). We also calculated two-phase compressibilities by using the same procedure, but with BO parameters given by the Batzle and Wang (1992) correlations, in which the only inputs are the specific gravities of the liquid and gas evolved from the fluid at standard conditions (equal here to 0.95 and 0.68, respectively): these compressibilities turn out to be undistinguishable from those calculated with the BO parameters.. In addition, we have depicted the more exact (adiabatic) compressibilities obtained by the method described in Nichita et al. (2010).

The discontinuous variation in fluid compressibility that occurs at the crossing of bubble point conditions is the most striking result of these calculations, whether performed by using the simple BO scheme introduced in this paper or by using the more rigorous scheme presented in the Nichita et al. (2010). Fluid compressibility jumps from a value approximately equal to 10^{-4} bar^{-1} just above P_b, i.e., in the one-phase (liquid) region (S_l=1, $P>P_b$), to a value four to five times larger (depending on the scheme used) in the two-phase region ($P<P_b$, S_l slightly below 1). This discontinuous variation, reminiscent of that well known in pure fluids

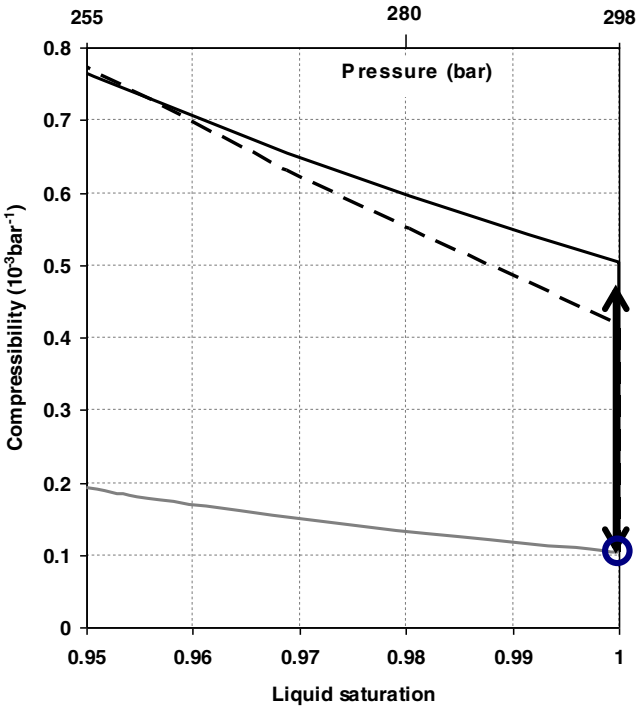

Fig. 1 Compressibility as a function of liquid saturation of the hydrocarbon fluid S_l at temperature T=344 K and pressure varying below bubble point pressure P_b=298 bar, calculated for "frozen" (or unrelaxed) liquid and gas phases (Wood's regime, *gray curve*) and for thermodynamically equilibrated (or relaxed) phases ("thermodynamic" or Landau–Lifshitz' regime). In the latter regime, compressibility is calculated either from BO parameters (*dashed curve*) or from an equation of state (*full black curve*). The *circle* on the axis S_l=1 corresponds to the compressibility of the one-phase (oil) system right above bubble point pressure. The *double arrow* shows the discontinuity in the compressibility of relaxed liquid and gas phases at the crossing of bubble point conditions

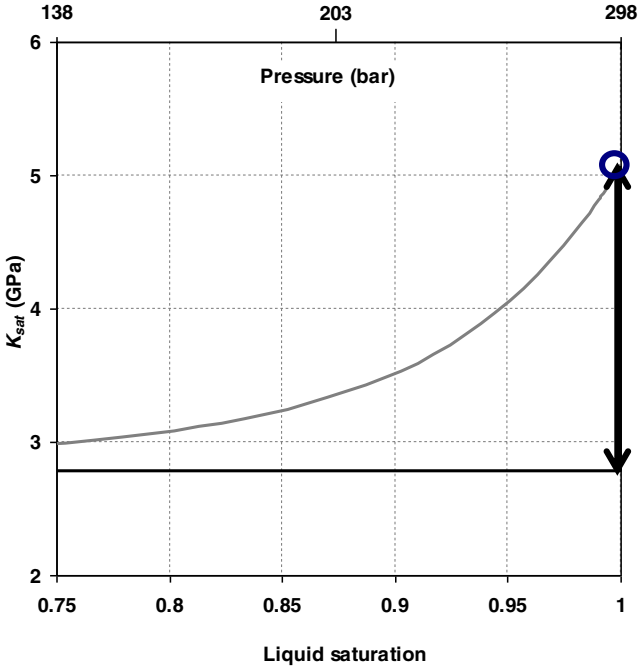

Fig. 2 Bulk modulus K_{sat} of the porous medium saturated with the hydrocarbon fluid considered in Fig. 1, computed by the Gassmann–Wood (GW) method (*gray curve*) and by the conventional Gassmann–Landau–Lifshitz (GLL) method (*full black curve*). The *circle* indicates the bulk modulus slightly above the bubble point pressure of the saturating fluid. The *double arrow* shows the discontinuity in the GLL modulus at the crossing of bubble point conditions

(Landau and Lifshitz 1959), is marked by the double arrow in Fig. 1. In contrast, the compressibility of "frozen" (or unrelaxed) oil and gas phases (i.e., Wood's compressibility, cf. Eq. 3) varies continuously at the crossing of bubble point conditions. Wood's (unrelaxed) two-phase compressibilities are much smaller than their "thermodynamic" (or relaxed) counterparts at low gas saturation.

We now examine the bulk modulus and P-wave velocity of the porous medium (whose parameters have been given above) saturated with the above hydrocarbon fluid. Indeed, we expect these two parameters to reflect the compressibility behavior of the saturating fluid, and in particular to exhibit a discontinuity at the crossing of bubble point conditions and much lower values at low gas saturation than the values obtained within the conventional Gassmann–Wood procedure. Injecting in Gassmann's substitution formula (Eq. 1) the fluid compressibilities calculated either within the "thermodynamic" (or Landau–Lifshitz) regime or within Wood's regime, and then using Eq. 2, we obtain the bulk moduli and P-wave velocities displayed in Figs. 2 and 3, respectively. We refer below to these two calculation methods as the Gassmann–Landau–Lifshitz (GLL) and GW methods. At very low gas saturation (S_g ~0 or S_l ~1), the GLL bulk modulus and P-wave velocity are lower by approximately 45 and 15 %, respectively, than their GW counterparts. The difference between the GLL and GW values decreases with increasing gas saturation and becomes very small when S_l<0.75 (Figs. 2 and 3).

CO_2-bearing aquifer

We consider here an aquifer homogeneously saturated with a small amount of "free" CO_2. This situation corresponds for example to an aquifer contaminated by CO_2 leaking from an underlying storage formation. In the early stages of leakage, CO_2 is dissolved in water, then a "free" CO_2-rich phase forms when the CO_2 dissolution limit is reached. This situation also corresponds to regions in the storage formation itself where "free" CO_2 is sparsely and homogeneously distributed in the porous medium, which is the case for instance in the region behind the rising CO_2 plume.

The porous medium is the same as that considered in the preceding example, with properties very close to those of the Utsira aquifer in the North Sea in which over 10 millions of tons of CO_2 have been injected since 1996. The temperature is equal to 335 K. The BO parameters of mixtures of water and CO_2 are easily found in the literature. For instance, values of R_s

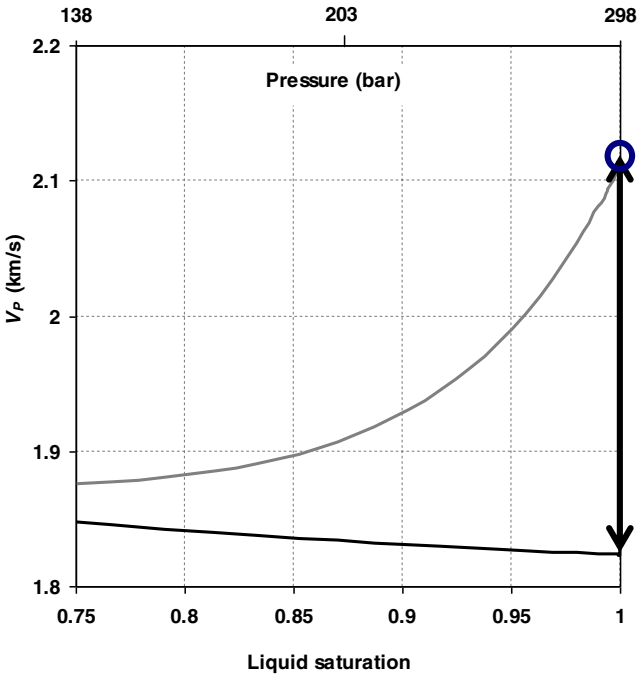

Fig. 3 P-wave velocity of the porous medium saturated with the hydrocarbon fluid considered in Fig. 1, computed by the GW method (*gray curve*) and by the GLL method (*black curve*). The circle indicates the P-wave velocity slightly above the bubble point pressure of the saturating fluid. The *double arrow* shows the discontinuity in the GLL P-wave velocity at the crossing of bubble point conditions

can be found in Chang et al. (1998) or in Hassanzadeh et al. (2008), and B_g is obtained by using the adaptation of the Batzle–Wang equations to CO_2 proposed by Xu (2006), which consists in using the true CO_2 critical temperature (T_c) and pressure (P_c) rather than the pseudo-T_c and pseudo-P_c drawn from the Batzle–Wang correlations. The "thermodynamic" (or relaxed) compressibilities of these mixtures are calculated in the one-phase (liquid) and two-phase (liquid and gas) regions by means of Eqs. 6 and 7. They are depicted as a function of liquid saturation varying between 0.98 and 1 in Fig. 4a, b. Figure 4a corresponds to varying pressure conditions (between P_b=178 bar and P=110 bar) at fixed fluid composition characterized by $R_s(P_b)$=27 l of CO_2 per liter of water at standard conditions (this value is nothing but the solubility of CO_2 in water at 178 bar and 335 K). Figure 4b corresponds to fixed temperature (335 K) and pressure (178 bar) and varying fluid compositions characterized by gas–water volume ratios larger than 27 l of CO_2 per liter of water (standard conditions). In these figures, the adiabatic compressibilities calculated by the method described in Nichita et al. (2010) are also depicted, which are not very different from those obtained within our simplified BO scheme. There is again at the crossing of bubble point

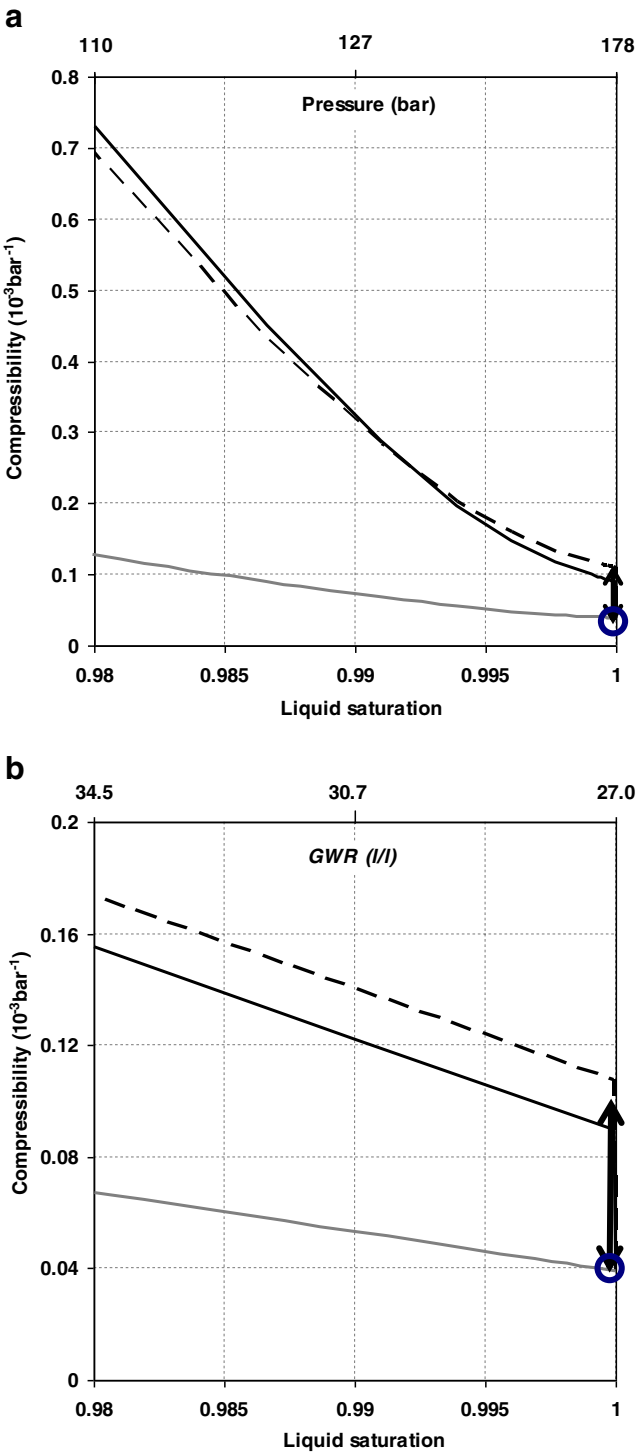

Fig. 4 **a** and **b** Compressibility as a function of liquid saturation of mixtures of water and CO_2 at T=335 K, calculated by assuming "frozen" (or unrelaxed) liquid and gas phases (Wood's regime, *gray curve*) and thermodynamically equilibrated (or relaxed) phases ("thermodynamic" or Landau–Lifshitz regime). In the latter regime, compressibility is calculated either from BO parameters (*dashed curve*) or from an equation of state (*full black curve*). The circle on the axis S_l=1 corresponds to the compressibility of the one-phase (liquid) CO_2-saturated water slightly above P_b=178 bar. The *double arrow* shows the discontinuity in the "thermodynamic" compressibility at the crossing of bubble point conditions. Figure 4a corresponds to a fixed composition and pressures varying below bubble point pressure P_b=178 bar. Figure 4b corresponds to varying compositions (or gas–water volume ratios, *GWR*, at standard conditions) at fixed P=178 bar

conditions a discontinuity in "thermodynamic" (or relaxed) compressibility, marked by the double arrow in Fig. 4a, b. This discontinuity is less pronounced than in the preceding example. Fluid compressibility is enhanced by a factor of 2.5 when this aqueous fluid turns biphasic, instead of a factor of 4–5 in the case of the hydrocarbon fluid examined above. In

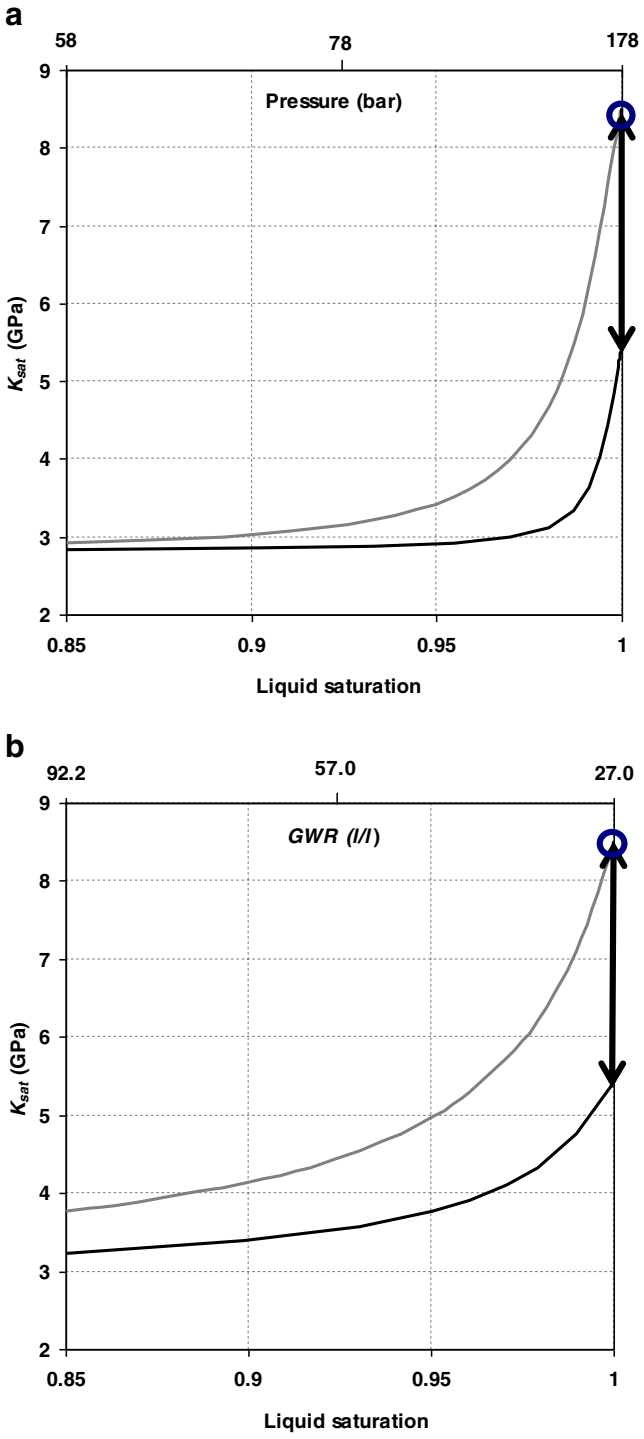

Fig. 5 **a** and **b** Bulk modulus K_{sat} of the porous medium saturated with the mixtures of water and CO_2 considered in Fig. 4a, b, respectively, computed by the GW method (*gray curve*) and by the GLL method (*black curve*). The circle indicates the bulk modulus of the reservoir rock saturated with the one-phase (liquid) CO_2-saturated water slightly above P_b=178 bar. The *double arrow* shows the discontinuity in the GLL bulk modulus at the crossing of bubble point conditions

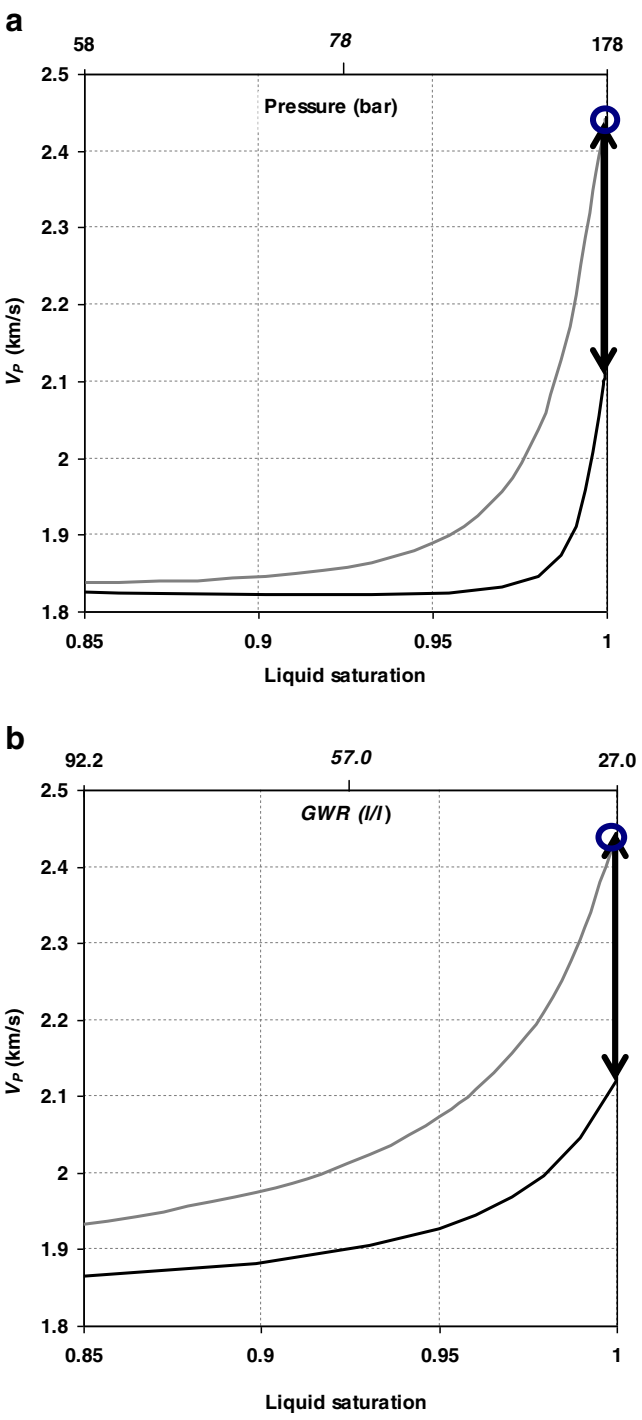

Fig. 6 **a** and **b** P-wave velocity in the porous medium saturated with the mixtures of water and CO_2 considered in Fig. 4a, b, respectively, computed by the GW method (*gray curve*) and by the GLL method (*black curve*). The *circle* indicates the P-wave velocity in the reservoir rock saturated with the one-phase (liquid) CO_2-saturated water slightly above P_b=178 bar. The *double arrow* shows the discontinuity in the GLL P-wave velocity at the crossing of bubble point conditions

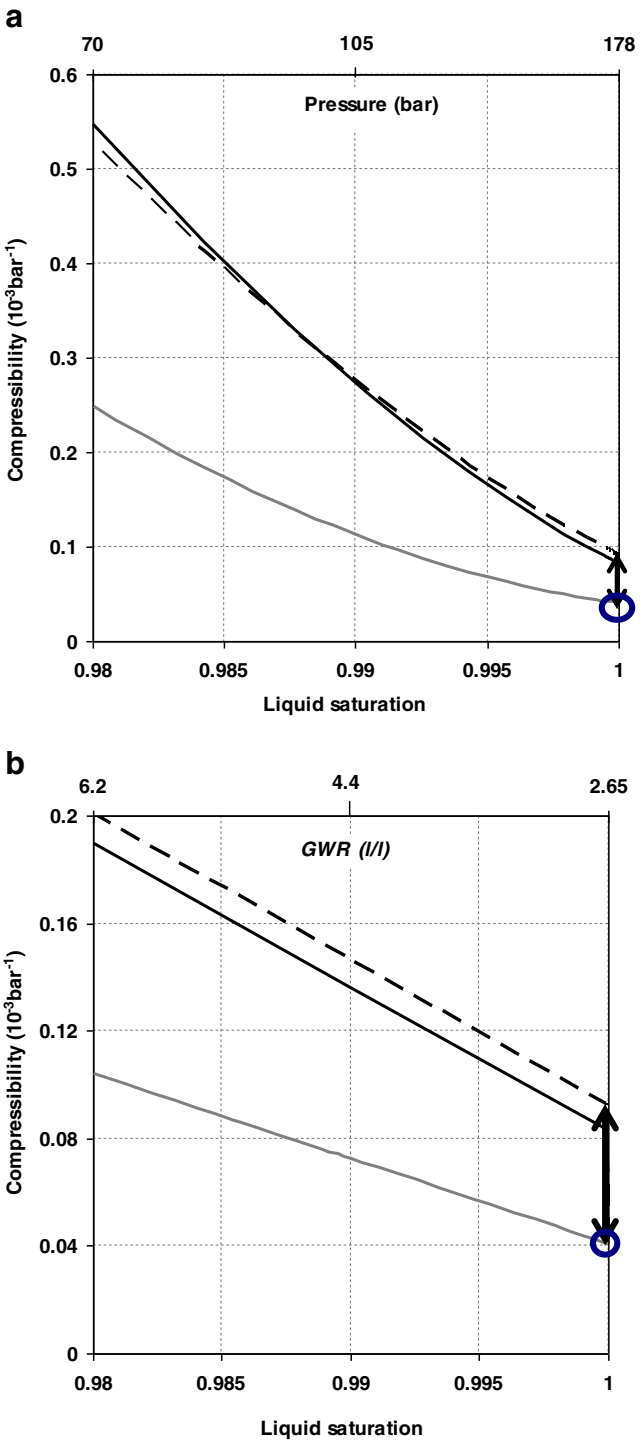

Fig. 7 **a** and **b** Compressibility as a function of liquid saturation of mixtures of water and CH_4 representative of "fizz" water, calculated by assuming "frozen" (or unrelaxed) liquid and gas phases (i.e., Wood's regime, *gray curve*) and thermodynamically equilibrated (or relaxed) phases (i.e., "thermodynamic" or Landau–Lifshitz regime, *black curve*). The circle on the axis S_l=1 corresponds to the compressibility of the one-phase (liquid) CH_4-saturated water slightly above P_b=178-bar (T=335 K). The *double arrow* shows the discontinuity in the "thermodynamic" compressibility at the crossing of bubble point conditions. Figure 7a corresponds to a fixed composition and pressures varying below bubble point pressure P_b=178 bar. Figure 7b corresponds to varying compositions (or gas–water volume ratios, *GWR*, at standard conditions) at fixed P=178 bar

contrast, Wood's (unrelaxed) compressibilities (Eq. 3), also plotted in Fig. 4a, b, vary continuously at the crossing of bubble point conditions, and are significantly smaller than their "thermodynamic" (or relaxed) counterparts.

The bulk moduli of the porous medium saturated with the above mixtures of water and CO_2 have been calculated by the GLL and GW methods, i.e., by injecting in Gassmann's formula (Eq. 1) the "thermodynamic" and Wood's compressibilities. They are depicted as a function of liquid saturation in Fig. 5, b, which correspond respectively to the fluid conditions of Fig. 4a, b. The P-wave velocities are shown in Fig. 6a, b. At very low gas saturation, the GLL bulk modulus and P-wave velocity are lower, respectively, by about 36 and 13 %, than their GW counterparts. As is apparent in Fig. 6a, b, the differences between both approaches decrease when gas saturation increases and becomes negligible when S_g is larger than around 5 % (fixed composition and decreasing pressure, Figs. 5a and 6a) and 15 % (varying composition and fixed pressure, Fig. 6a, b). These differences are significant at low gas saturation, yet they are less pronounced, both in amplitudes and in saturation extent, than in the preceding example.

Fizz water-bearing reservoir

In this last example, illustrative of a reservoir saturated with fizz water, the porous medium, temperature and bubble point conditions are identical to those of the preceding example. The light component that is mixed with water is methane (CH_4) instead of CO_2. At 178 bar and 335 K, the solubility of CH_4 in water is 1 order of magnitude below that of CO_2: 2.7 l of CH_4 *vs*. 27 l of CO_2 per liter of water at standard conditions. We envisage again two situations: (a) one in which pressure varies below bubble point pressure P_b (=178 bar) at fixed fluid composition and (b) the other in which fluid composition varies at fixed pressure (equal to P_b).

The "thermodynamic" (or relaxed) compressibilities of these fluids calculated in the one-phase (liquid) and two-phase (liquid and gas) regions by means of Eqs. 6 and 7 are depicted as a function of liquid saturation varying between 0.98 and 1 in Fig. 7a, b, corresponding respectively to situations (a) and (b) described in the preceding paragraph. The values of $R_s(P)$ or $\partial R_s/\partial P$ used in this calculation have been found in Ramey (1964) or in Batzle and Wang (1992), who also provide a method for estimating the volume factors B_g and B_w of pure methane and water (these factors can also be inferred from the NIST data base). These compressibilities are very close to the adiabatic compressibilities computed by the method described in Nichita et al. (2010). The discontinuity in

"thermodynamic" (or relaxed) compressibility at the crossing of bubble point conditions (S_l=1), marked by the double arrow in Fig. 7a, b, is smaller than in the case of the water+CO_2 systems with identical bubble point temperature and pressure. Fluid compressibility is enhanced by a factor of 2 when the first bubble of *free* CH_4 appears in the aqueous

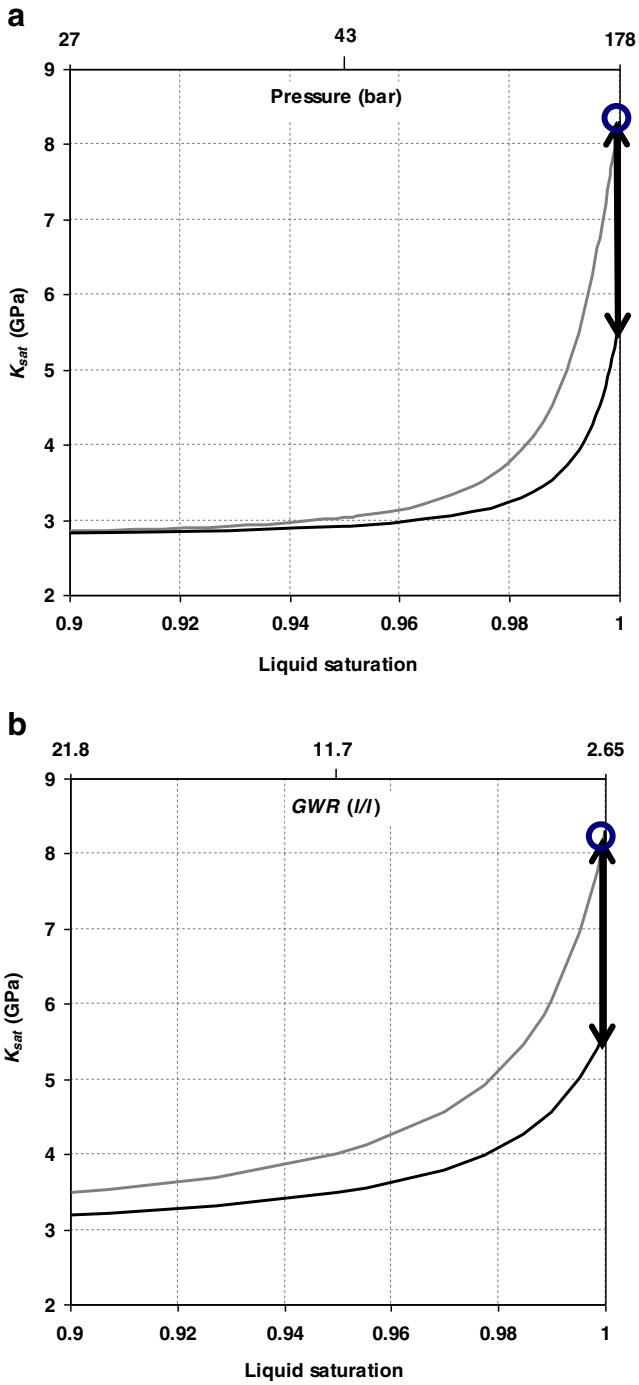

Fig. 8 **a** and **b** Bulk modulus K_{sat} of the porous medium saturated with the "fizz" water considered in Fig. 7a, b, respectively, computed by the GW method (*gray curve*) and by the GLL method (*black curve*). The *circle* indicates the bulk modulus of the reservoir rock saturated with the one-phase (liquid) CH_4-saturated water slightly above P_b=178 bar. The *double arrow* shows the discontinuity in the GLL bulk modulus at the crossing of bubble point conditions

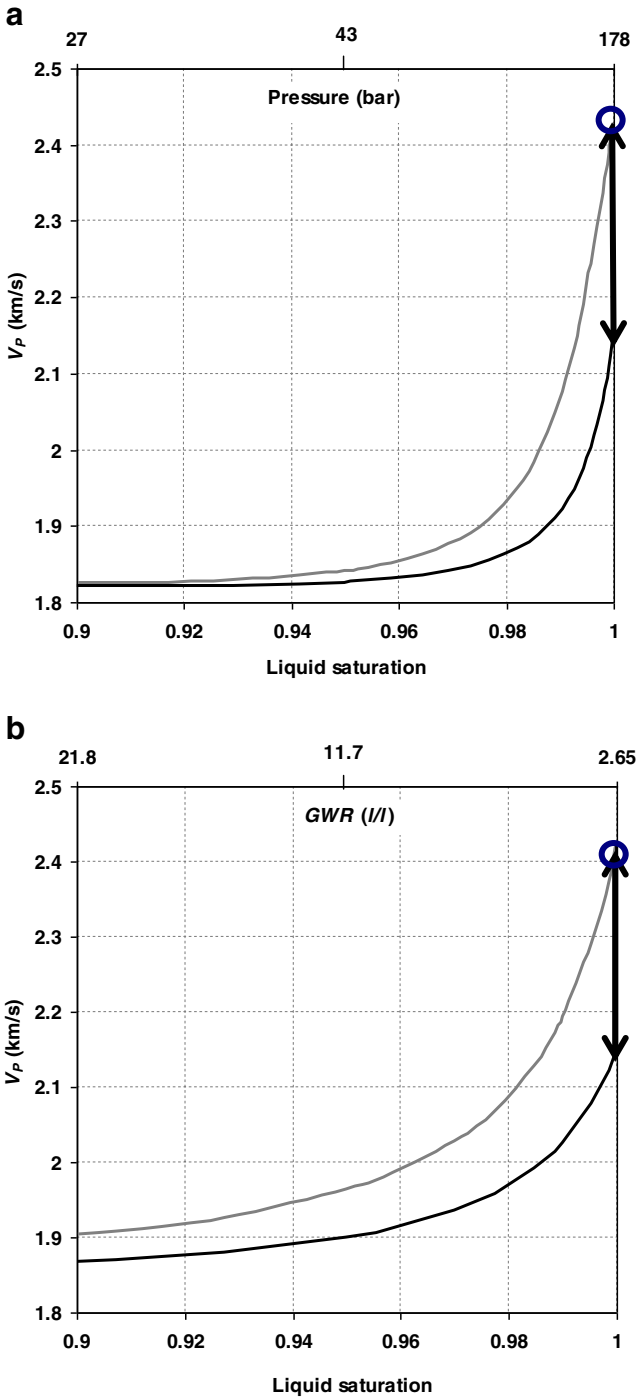

Fig. 9 **a** and **b** P-wave velocity in the porous medium saturated with the "fizz" water considered in Fig. 7a, b, respectively, computed within the GW method (*gray curve*) and by the GLL method (*black curve*). The *circle* indicates the P-wave velocity in the reservoir rock saturated with the one-phase (liquid) CH_4-saturated water slightly above P_b=178 bar. The *double arrow* shows the discontinuity in the GLL P-wave velocity at the crossing of bubble point conditions

phase. In contrast, Wood's compressibilities (Eq. 3) vary continuously at the crossing of bubble point conditions and are smaller than their "thermodynamic" (or relaxed) counterparts.

The GLL and GW bulk moduli of the porous medium saturated with this fizz water are depicted as a function of liquid saturation in Fig. 8a, b, corresponding respectively to the fluid conditions of Fig. 7a, b. The P-wave velocities are shown in Fig. 9a, b. At low gas saturation, the GLL bulk modulus and P-wave velocity are lower by ~32 and 12 %, respectively, than their GW counterparts. The differences between both approaches decrease when gas saturation increases and become negligible when S_g is larger than about 4 % (situation a) and 10 % (situation b). These differences are less pronounced than those obtained with CO_2, which is again an effect of the lesser solubility in the saturating liquid (i.e., water) of methane as compared to CO_2.

Discussion and conclusions

The previous analysis shows that the drops in bulk modulus and P-wave velocity caused by small gas saturation in a liquid-bearing porous medium are likely to be underestimated by the conventional Gassmann–Wood approach, in which the effects of phase changes between liquid and gas are neglected. As shown above from a simple argument valid for low pressures (Eq. 10) and from calculations with reservoir examples, this underestimation is more important, both in amplitude and saturation extent, for liquid/gas systems in which gas solubility in the liquid is higher. The difference between the GW and GLL velocities (and impedances) is thus larger when the reservoir fluid is a live oil with a small amount of gas than when it is water with gas, and in the latter aqueous systems when the gas is CO_2 rather than methane.

We expect this difference to be apparent in the seismic traces of low gas-saturated reservoirs. We focus in this preliminary analysis on normal (zero offset) reflections, which are known to be the most sensitive to the value of V_P. We defer to a subsequent work a more complete AVO analysis. The synthetic seismic traces correspond here to a 40 Hz Ricker wavelet, impinging on a 100 m thick reservoir layer encased in shales with density 2.27 g/cm^3 and V_P=2.4 km/s, convolved with the reflectivity coefficient profiles at zero-offset conditions. They have been calculated for the three reservoir examples with various low gas saturations described in the previous section. Depending on whether the GW or GLL methods are used for modeling velocities and impedances, very different seismograms are expected as a consequence of the difference between the zero-offset reflectivities, or impedance contrasts, at reservoir/shale interfaces. Figure 10 represents vertical impedance profiles of the chosen shale/reservoir geological setting, in which the reservoir is fully saturated with liquid (oil or water) and partially saturated with gas (S_g=0.01). The liquid/gas systems and the temperature and pressures are those considered in the previous section (Figs. 1, 4a, and 7a). The corresponding traces are plotted in Figs. 11 and 12. The traces corresponding to S_g=0.05 are also plotted in Fig. 11. Clearly, reflection amplitudes at shale/reservoir interfaces are larger when calculated by using the GLL velocity model rather than the GW model, especially at lower saturation (S_g=0.01) and when the gas is CO_2 (Fig. 11). This difference however decreases with increasing gas saturation, as shown for instance in Fig. 10 (hydrocarbon-bearing reservoir). Upon further approaching bubble point conditions (i.e.,

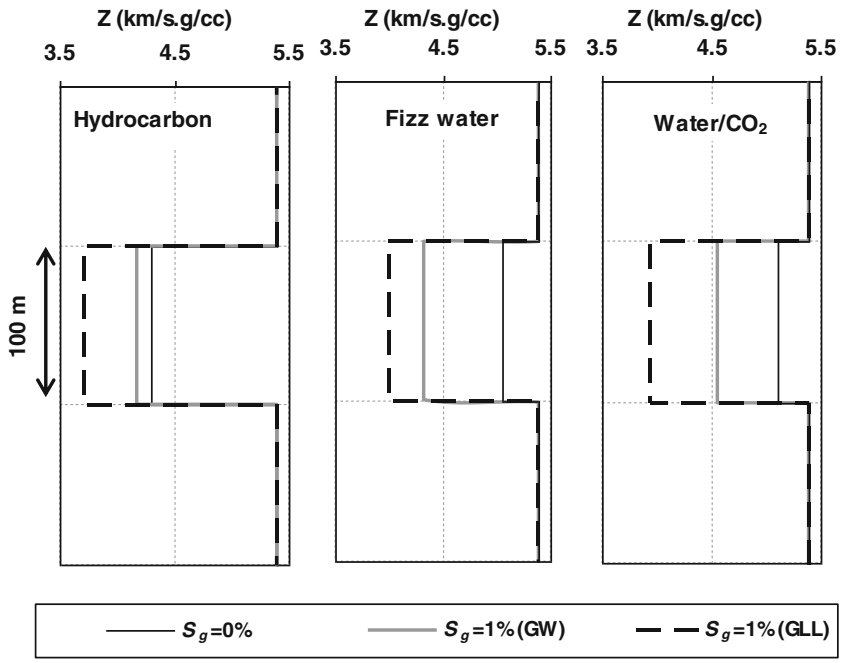

Fig. 10 Vertical profiles of the GW and GLL P-wave impedance of the shale/reservoir geological setting, corresponding to reservoirs fully liquid saturated (S_g=0) and partially saturated with gas (S_g=0.01). The fluid systems are those considered in Figs. 1, 4a, and 7a

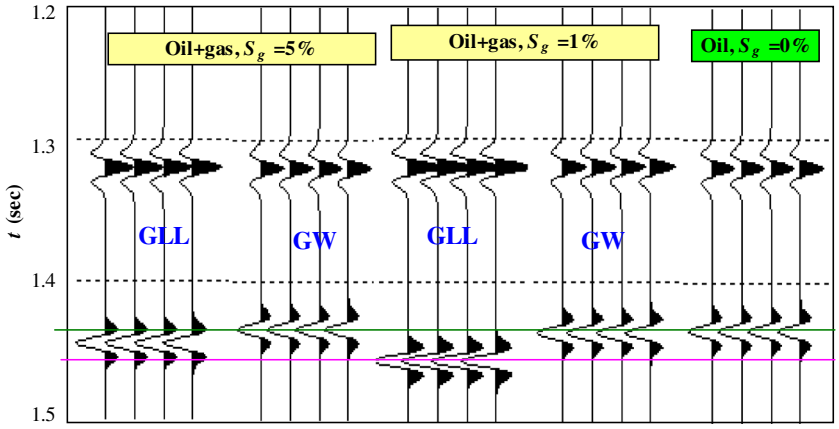

Fig. 11 Zero-offset synthetic seismic traces of a shale-encased 100 m thick hydrocarbon-bearing reservoir layer with various low gas saturations: S_g=0.05, 0.01, 0 (from *left* to *right*). The poroelastic properties given by the GLL and GW models are plotted in Fig. 10

S_g<0.01) in those formations, the GLL traces are almost unchanged from their values for S_g=0.01, whereas the GW traces tend to the traces of the corresponding fully liquid-saturated formation (data not shown here). For values of S_g exceeding about 0.1, the differences between the GW and GLL amplitudes are hardly detectable (data not shown). Another interesting feature of these traces is the stronger velocity pushdown effect at the bottom reservoir/shale interface obtained when using the GLL velocity model compared to the effect obtained when using the GW model. For a given low gas saturation, the pushdown effect is larger when the gas is more soluble.

The GLL method introduced in this paper is valid at "low enough" frequency, corresponding to thermodynamically equilibrated (or relaxed) liquid and gas phases saturating the porous rock. The conventional GW model holds if the frequency is "high enough", corresponding to "frozen" (or unrelaxed) liquid and gas phases. As argued above, the characteristic frequency f_c delineating the two frequency regimes is likely to fall in the seismic band for typical low gas-saturated reservoirs, and therefore dispersion–attenuation effects may occur in practice, with a frequency dependent P-wave (phase) velocity having values intermediate between the GLL and GW velocity values and an associated attenuation (by virtue of Kramers–Krönig relation). An extension of this work would be to examine both from a theoretical point of view and experimentally how these effects, which have been thoroughly investigated in pure bubbly fluids (Onuki 1991; Coste et al. 1992), compare and add up to the other acoustic dispersion-attenuation mechanisms (Bourbié et al. 1987).

According to our analysis, even minute amounts of "free" gas corresponding to the immediate vicinity of bubble point conditions in the reservoir should give rise to strong seismic reflections (bright spots). Interfaces between two porous layers, one fully saturated with liquid and the other with the same liquid with a minute amount of gas, should thus be associated to seismic reflectors. This kind of reflectors, associated to a phase change between a monophasic liquid and a two-phase (liquid and gas) fluid in the reservoir, is analogous to the so-called bottom simulating reflectors associated to another type of phase transition, namely that between a solid (hydrate) phase and a two-phase (water and gas) fluid. As another example, the 400–700 km deep reflectors observed at seismological frequencies (<1 Hz) have recently been shown to be associated to pressure-induced phase transitions in the earth's minerals (Li and Weidner 2008). The reflectors of interest in this paper, when

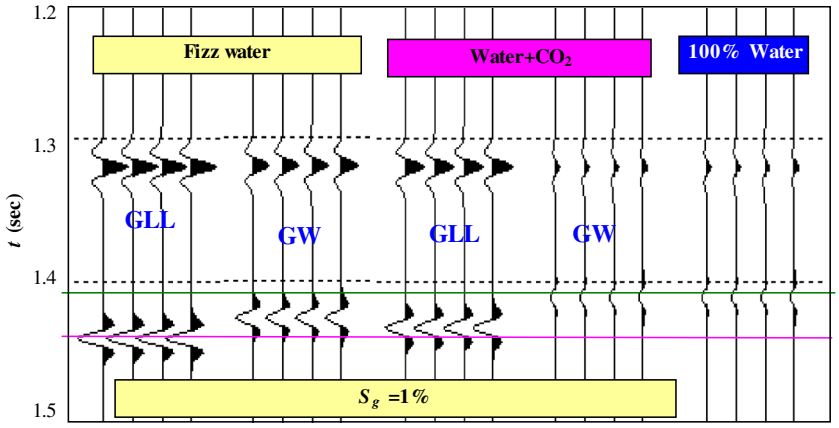

Fig. 12 Zero-offset synthetic seismic traces of a shale-encased 100 m thick fizz water-bearing and water/CO_2-bearing reservoir layer. The poroelastic properties given by the GLL and GW models (the impedance vertical profiles for S_g=0.01 and 0) are plotted in Fig. 10

they appear in time lapse seismic studies of a producing hydrocarbon reservoir are the manifestation of the crossing of bubble point conditions in the reservoir. In some aquifers containing dissolved methane, the solubility of which often goes through a minimum as a function of depth in off-shore conditions (Haacke et al. 2007), depletion may cause the apparition of a horizontal gas bubble curtain at the location of this minimum, which should also be clearly apparent in time lapse seismic studies.

In the context of the rising interest for CO_2 geological storage, our suggestion is to utilize the strong sensitivity of seismic velocity to very low saturations of free CO_2 (see, e.g., Fig. 6a, b) for monitoring purposes, not only of the plume CO_2 frontiers (where S_g has a nonvanishing values), and also of shallow aquifers overlying the storage formation. The contamination of the latter aquifers by CO_2 leaking from the storage formation could be detected as soon as CO_2 reaches the solubility limit, i.e., as soon as it forms a free phase in the shallow aquifer.

As mentioned in the "Introduction" section, discriminating between "fizz" water and commercial gas saturation is one of the most important challenges in seismic exploration. The conventional Gassmann–Wood method predicts that the P-wave velocity and impedance strongly vary with gas saturation only in a narrow interval, from S_g=0 to S_g=5–10 %, depending on reservoir depth. This strong variation is very likely to be overestimated, as demonstrated in this paper (see Fig. 9a, b); there is thus less hope to infer gas saturations from seismic reflectivity, since even a minute amount of free gas gives rise to an impedance contrast with the fully liquid-saturated zone comparable to that with a commercial gas saturation.

Acknowledgments This research has been partially supported by Agence Nationale de la Recherche under the project EMSAPCO2. The authors are grateful to François Montel (Total) for helpful discussions.

References

Arts R, Eiken O, Chadwick A, Zweigel P, van der Meer L, Zinszner B (2004) Monitoring of CO_2 injected at Sleipner using time-lapse seismic data. Energy 29:1383–1392

Batzle M, Wang Z (1992) Seismic properties of pore fluids. Geophysics 57:1396–1408

Bourbié T, Coussy O, Zinsner B (1987) Acoustics of porous media. Technip, Paris

Chang Y-B, Coats BK, Nolen JS (1998) A compositional model for CO2 floods including CO2 solubility in water. SPE Res Eval Eng 1(2):155–160

Coste C, Laroche C (1993) Acoustic behavior of a liquid/vapor mixture in a standing wave tube. J Fluid Mech 246:67–89

Coste C, Laroche C, Fauve S (1992) Acoustic resonances in a liquid with vapor bubbles: effect of liquid–vapor transition on sound velocity and attenuation. Phys Rev Lett 69:765–768

Firoozabadi A, Pan H (2000) Two-phase isentropic compressibility and two-phase sonic velocity for multicomponent-hydrocarbon mixtures. SPE Reserv Eval Eng 3:335–341

Gassmann F (1951) Uber die Elastizitat poroser Medien. Vierteljahrsschrift der Naturforschenden Gesellschaft in Zurich 96:1–23

Haacke RR, Westbrook GK, Hyndman RD (2007) Gas hydrate, fluid flow and free gas: formation of the bottom-simulating reflector. Earth Planet Sci Lett 261:407–420

Han D, Batzle M (2002) Fizz water and low gas-saturated reservoirs. Leading Edge 21:395–398

Han D, Batzle M (2004) Gassmann's equation and fluid-saturation effects on seismic velocities. Geophysics 69:398–405

Hassanzadeh H, Pooladi-Darvish M, Elsharkawy AM, Keith DW, Leonenko Y (2008) Predicting PVT data for CO_2—brine mixtures for black-oil simulation of CO2 geological storage. Int J Greenhouse Gas Control 2:65–77

Kieffer SW (1977) Sound speed in liquid–gas mixtures: water–air and water–steam. J Geophys Res 82:2895–2904

Landau LD, Lifshitz EM (1959) Fluid mechanics. Pergamon Press, Oxford

Li L, Weidner J (2008) Effect of phase transitions on compressional-wave velocities in the earth's mantle. Nature 454:484–486

McCain WD Jr (1990) The properties of petroleum fluids. Penn Well, Oklahoma

Nichita DV, Broseta D, Leibovici CF (2007) Reservoir fluid applications of a pseudo-component delumping new analytical procedure. J Pet Sci Eng 59:59–72

Nichita DV, Khalid P, Broseta D (2010) Calculation of isentropic compressibility and sound velocity in two-phase fluids. Fluid Phase Equilibria 291(1):95–102

Onuki A (1991) Sound propagation in phase-separating fluids. Phys Rev A 43:6740–6755

Peng DY, Robinson DB (1976) A new two-constant equation of state. Ind Eng Chem Fundam 15:59–64

Picard DJ, Bishnoi PR (1987) Calculation of the thermodynamic sound velocity in two-phase multicomponent fluids. Int J Multiphase Flow 13:295–308

Ramey HJ Jr (1964) Rapid methods for estimating reservoir compressibilities. J Pet Technol 16:447–454

Stenby EH, Christensen JR, Knudsen K, Leibovici CF (1996) Application of a delumping procedure to compositional reservoir simulations, SPE 36744, the SPE Annual Technical Conference and Exhibition held in Denver, CO, October 6–9

Temkin S (1992) Sound speed in suspension in thermodynamic equilibrium. Phys Fluids A 4:2399–2409

Trammell GT (1962) Sound speed in water containing vapor bubble. J Appl Phys 33:1662–1670

Wood AW (1930) A textbook of sound, 1st edn. Macmillan, New York

Xu H (2006) Calculation of CO_2 acoustic properties using Batzle–Wang equations. Geophysics 71:F21–F23

Zinszner B, Pellerin FM (2007) A geoscientist's guide to petrophysics. Technip, Paris